Ocean and Coastal Research

ORIGINAL ARTICLE

http://doi.org/10.1590/2675-2824070.22033mbc
ISSN 2675-2824

Wave climate and extremes on a mesotidal atoll lagoon

Mirella B. Costa[1,2], Eduardo Siegle[3,*]

[1] Universidade de São Paulo - Instituto Oceanográfico - Programa de Pós-Graduação em Oceanografia (Praça do Oceanográfico,191 - São Paulo - 05508-120 - SP - Brazil)
[2] Universidade Federal de Pernambuco - Departamento de Oceanografia (Rua da Arquitetura, sn - Recife - 50740-550 - PE - Brazil)
[3] Universidade de São Paulo - Instituto Oceanográfico (Praça do Oceanográfico,191 - São Paulo - 05508-120 - SP - Brazil)

* Corresponding author: mirella.costa@ufpe.br

ABSTRACT

Processes on atolls and coral reef lagoons are defined by local wave and tide climates. Based on the reconstruction of lagoon wave climate by downscaling offshore historical wave information, this study aims to assess the wave climate and wave extremes on a mesotidal atoll lagoon (Rocas Atoll, Brazil). Results show that the transformation of offshore waves, when propagating into the lagoon, results in a different and far more homogeneous wave climate. Atoll morphology and tides play a key role in controlling the directional and energy characteristics of the lagoon wave climate. Refraction processes and the reef passage make the side protected from the dominant SE waves the most energetic zone for lagoon wave propagation. Lagoon waves tend to propagate in opposite directions to offshore wind waves, showing the refraction effect of approaching waves when crossing the atoll rim and the channel. The tidal effect on the dissipation process is also a filter for extreme wave conditions. We highlight the dependence of the resulting lagoon wave climate on atoll morphology, thereby addressing its implications to geomorphological process inside the atoll.

Descriptors: Wave propagation, Reef wave transformation, Rocas Atoll.

INTRODUCTION

Geomorphic and ecological processes on atolls and coral reef lagoons are closely linked to local wave and tide regimes (Woodroffe and Biribo 2011). As waves approach a reef and break, they generate a rise in the dynamic sea level relative to the offshore mean sea level, initiating water transport across the rim towards the lagoon (Atkinson et al. 1981; Tartinville et al. 1997; Kraines et al. 1999; Lowe and Falter 2015). The directions of these wave-induced currents will depend on the swell and wind wave direction, as well as on the wave refraction controlled by the reef morphology (Costa et al. 2019). The side facing the largest waves will have large amounts of water pushed over the reef rim, while water will drain to the ocean on the leeward side (Callaghan et al. 2006). This process may be modulated by tides (Costa et al. 2017a).

The combination of tide and wave-driven flows through the rim are critical for ecological functions of reef systems, such as renewal of water and oxygen and their uptake by corals (Jokiel 1978; Nakamori et al. 1992; Hearn et al. 2001), removal of metabolic waste and flushing of reef lagoons (Frith and Mason 1986; Kench 1998a; Dumas et al. 2012), and the dispersal and recruitment of larvae (Hamner and Wolanski 1988; Black 1993; Abelson and Denny 1997). However, depending

Submitted: 12-April-2022
Approved: 24-May-2022

Associate Editor: Piero Mazzini

on the local tidal setting, not all wave energy will be dissipated at the reef edge at high tide (Kench et al. 2006). Instead, waves may propagate onto the reef surface either as transformed incident waves, reformed waves, or wave bores (Nelson 1996; Lugo-Fernández et al. 1998). The wave energy that leaks onto coral reef surfaces is critical in activating the geomorphic processes of sediment transport and in governing reef island construction and its morphological changes (Gourlay 1988; Roberts et al. 1992; Kench 1998b; Brander et al. 2004).

Large scale numerical hindcast modelling has provided continuous time series of offshore wave parameters over significant periods of time (Chini et al. 2010), allowing for the consistent description of the wave climate and extreme wave analysis in locations where instrumental data are unavailable (Camus et al. 2013). These types of models have been used to define offshore wave climate and extremes. However, waves are poorly described in shallow areas due to the insufficient spatial resolution and because wave transformations, due to the interaction with the complex bathymetry, are not typically modeled (Camus et al. 2013).

Downscaling is a method to obtain information at high spatial resolutions from relatively coarse data (Camus et al. 2011). High-resolution wave models can be used to downscale the historical wave climate from hindcast models and to reconstruct the spatial wave fields in shallow water, where depth variations and local bathymetry are important variables for wave transformation processes. This technique has been applied to coastal environments (Camus et al. 2011, 2013; Charles et al. 2012a, b) to reproduce their wave climate and their relation to nearshore processes. However, few applications are found for atolls (e.g. Amores et al. 2021), although significant differences are observed between the offshore and lagoon wave climates. This is due to high wave attenuation upon crossing the shallow reef rim. Tides play a key role in this process, controlling the water level above the reef and modulating the amount of energy that can be transmitted through the atoll rim (Brander et al. 2004; Beetham and Kench 2014; Beetham et al. 2016). Thus, the definition of extreme conditions inside the lagoon may be directly related not only to the extreme conditions of offshore waves, but also, and especially, to the joint occurrence with high tides.

Through the reconstruction of lagoon long-term time series by downscaling offshore historical wave climate, this study aims to assess the wave climate and wave extremes analysis on a mesotidal atoll lagoon (Rocas Atoll). This step involves the implementation and validation of a high-resolution wave propagation model. Moreover, this study addresses the joint occurrence of energetic wave conditions and high tides and the implications of the differences on the offshore and lagoon wave climates to geomorphological process inside the atoll.

METHODS

Study area

Rocas is the only atoll in the South Atlantic Ocean (3.863° S, 33.804° W) and a strictly regulated Brazilian nature reserve limited to scientific research, environmental monitoring, and education since 1979 (Figure 1). Located slightly south of the Equator, Rocas Atoll is outside of the tropical storm belt. The atoll is dominated by the southeast trade winds, which prevail for 93% of the year (BDC 2015), varying in strength according to the Intertropical Convergence Zone (ITCZ) seasonality (McGregor and Nieuwolt 1998). The average wind speed is ~5 $m.s^{-1}$, with a maximum speed of ~11 $m.s^{-1}$ (BDC 2015). North- and southward-directed swells also contribute to the wave conditions at Rocas, generated during the winter of each hemisphere (Costa et al. 2019). Wave energy in the lagoon is at least one order of magnitude lower than offshore wave energy and is strongly modulated by tides (Costa et al. 2019). Significant wave height measured from in situ equipment ranges from 0.01 to 0.81 m, with maximum values during high spring tides (Costa et al. 2017a). The lagoon wave spectrum is dominated by both infragravity wave energy (>0.05 Hz) and wind wave energy (0.333–0.125 Hz) (Costa et al. 2017a).

Due to its shallow lagoon and continuous reef rim, interrupted only by two reef passages, Rocas is similar to an elliptical platform reef (e.g., Gourlay 1988; Mandlier and Kench 2012) in terms of wave

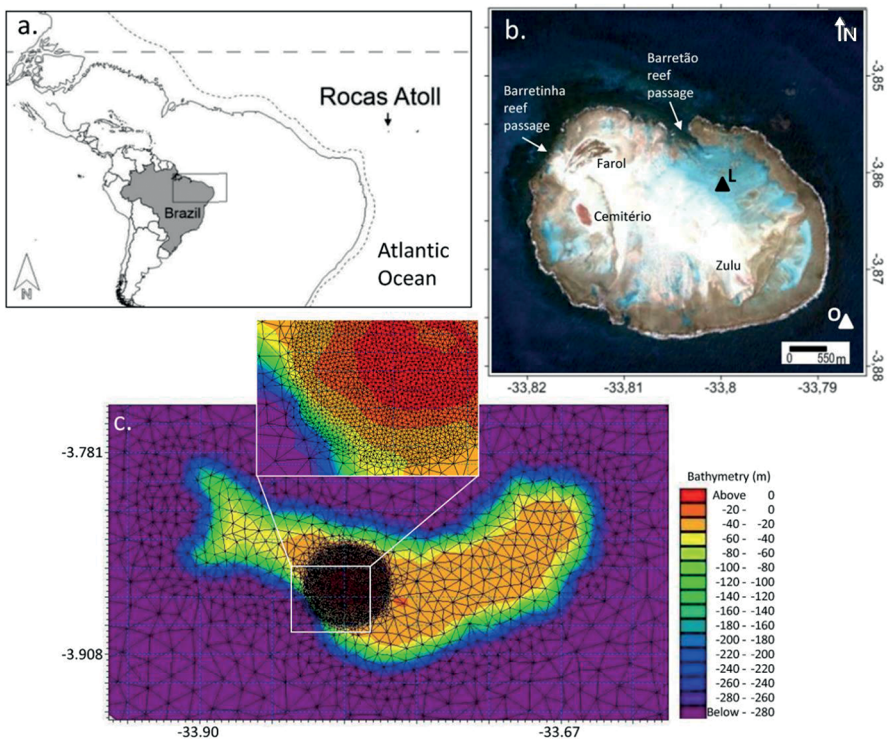

Figure 1. a. Location of the Rocas Atoll; b. Image (Google Earth Pro) of the atoll with the indication of main features and triangles indicating the lagoon (L) and offshore (O) ADCP moorings; c. numerical model mesh and bathymetry.

refraction patterns (Costa et al. 2019). Wave vectors converge mainly on the leeward side, and an interference zone exists on the windward side through the lagoon. The larger reef passage controls the location of the convergence zone by allowing offshore waves from different directions to penetrate into the lagoon with less dissipation (Costa et al. 2019).

The only two reef islands on the leeward reef are typical sand cays composed mainly of sands (Figure 1). Farol island is horseshoe shaped, with a series of asymmetric low-elevation ridges and a central depression (Costa et al. 2017b). This depression is flooded during high tides, and its pit lies at almost the same level as the surrounding reef flat (1.9 m above MLWS). Cemitério Island has an elongated planform shape, with only slight asymmetry between the oceanward (5m above MLWS) and lagoonward ridges (4.5 m above MLWS). The lagoonward side is completely surrounded by exposed consolidated sediments (beachrock or cay sandstones) (Costa et al. 2017b). Rocas also exhibits a shingle bank on the windward side, as expected for an elliptical platform formed by material transported from the windward reef rim by occasional energetic swells generated by mid and high-latitude storms (Costa et al. 2017b).

Local tides are semi-diurnal, with an ocean tidal range of 2.8 m during spring tides and 1.7 m during neap tides (Costa et al. 2017a). Circulation in the Rocas lagoon is wave-driven and controlled by tides (Costa et al. 2017a). Waves breaking on the windward reef rim pump water into the lagoon, causing a consistent westward flow through the atoll and outflow at the reef passages. During low tides, the wave pumping mechanism is blocked by the vertical exposure of the reef rim, causing flow reversion at the large reef passage (Costa et al. 2017a).

Wave data

The wave climate was characterized using data from available global models and applying a local wave propagation model. The strategy consisted of statistically analyzing the wave time series extracted from the global model to represent the incident wave climate (offshore) and reconstructing this series through a local model to represent the waves

in the atoll lagoon, considering the transformation processes and tidal effects as they propagate onshore (Figure 2).

Global model

The wave climate analysis of Rocas Atoll was performed using data from the global wave generation model WAVEWATCH III (NWW3) version 2.2, developed by the National Oceanic and Atmospheric Administration/National Centers for Environmental Prediction (NOAA/NCEP; Tolman 2002). The model is forced with wind fields produced by the global atmospheric model Global Forecast System (GFS) and solves the wave action spectral density conservation equation to generate global domain spectral and wave characteristics data. The data are available at 3 h intervals with 0.5-degree spatial resolution. The NWW3 hindcast data was extracted at the nearest grid point and covers 35 years, from 1979 to 2014.

Local model

To evaluate the wave climate for Rocas lagoon with high temporal and spatial resolution, the offshore wave data from NWW3 were downscaled using the third-generation wave model MIKE21 SW. MIKE21 SW numerically solves the wave action conservation equations, with discretization performed using a cell-centered, finite volume approach that simulates the transformation of random, short-crested surface waves (Holthuijsen et al. 1989; Sørensen et al. 2004). The model estimates the transformation of incident wave energy by shoaling, refraction, diffraction, and dissipation by both depth-induced wave breaking and bottom friction. The domain and the governing equations

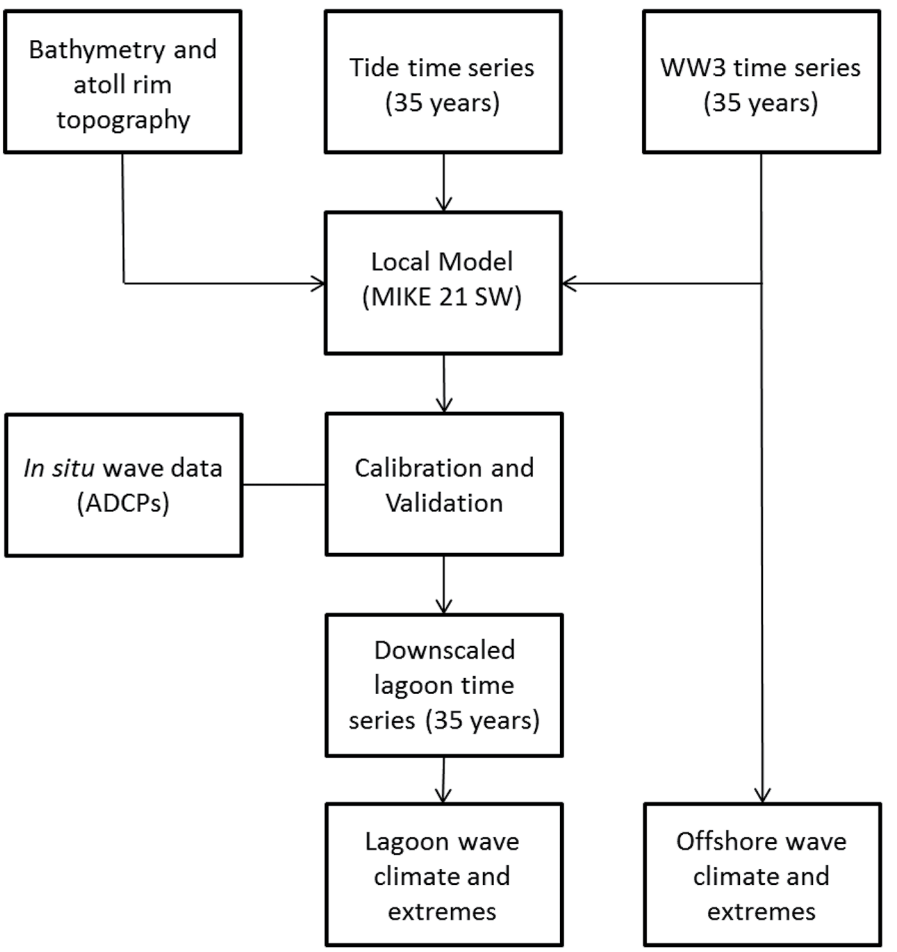

Figure 2. Global framework to obtain offshore and lagoon wave databases.

are discretized using the finite volume method. The model is quasi-stationary using a Runge-Kutta iterative procedure to compute the stationary wave field at each time step (Sørensen et al. 2004).

An unstructured mesh containing 6953 triangular elements with varying resolution was used (Figure 1). A fine grid (~60 m spatial resolution) covers the atoll area and is connected to the lower offshore resolution of ~1.5 km by an intermediate resolution grid (cells of ~600 m). The long-term time series from NWW3 was used as a forcing condition for the local model that contains the detailed bathymetry and morphology of the Rocas Atoll and surrounding shelf. The description of model configuration and the topo-bathymetric dataset used in this study can be found in Costa et al. (2019).

The tidal variation time series for the analyzed period (1979 to 2014) was also used as a boundary condition to reconstruct the wave climate inside the lagoon. This time series was reproduced using the tidal harmonic constants extracted from measured sea level variation collected at Fernando de Noronha Archipelago (~140 km away), encompassing 611 sampling days at 60 min intervals, totaling 14,664 heights recorded. These data were provided by the national oceanographic database of the Brazilian navy (Banco Nacional de Dados Oceanográficos da Marinha do Brasil).

Definition of wave climate and extremes

The lagoon and offshore wave climate of Rocas Atoll was defined by analyzing the seasonality and extremes events based on the time series from 1980 to 2014. Directional wave climatologies were constructed by discretizing wave parameters Hs and Tp into 0.5 m and 2 s, respectively, by 45° peak wave direction (θp) bins that correspond to the 8 wave direction octants (N, NE, E, SE, S, SW, W, NW). These binned values were then analyzed for the most frequent occurrences of Hs and Tp (typical conditions) and the 99th percentiles (maximum condition). This method allows for an examination of how often (in a year or season) a particular wave direction/frequency event tends to occur and its average magnitude (Hoeke et al. 2011).

Considering that the greatest wave heights are not necessarily associated with the highest wave periods, and that the combination of both high values corresponds to the highest wave energy events, the wave power was calculated to classify the swell intensity and characterize extreme events. The wave power (P, expressed as kW/m) correlates Hs and Tp through the product between group velocity (Cg) and wave energy (E), resulting in:

$$P = \frac{\rho g^2 H^2 T}{64\pi}, \quad (1)$$

where ρ is the water density (1027 kg/m^3) and g is the acceleration due to gravity.

High values of both parameters (Hs and Tp) are associated with energetic events capable of causing significant changes in local morphology. This equation is used to define the swell intensity classes that reach Rocas Atoll, according to the intervals listed in Table 1.

Table 1. Wave intensity classification based on wave power.

Intensity	Wave Power (kW/m)
Extreme	$P \geq 50$
Severe	$50 > P \geq 40$
Strong	$40 > P \geq 30$
Moderate	$30 > P \geq 20$
Weak	$20 > P \geq 10$
Calm	$P < 10$

Local model validation

The local model applied in this study is the same as in Costa et al. (2019), validated using the time series recorded by two Acoustic Doppler Current Profilers (ADCPs) deployed for 28 days on Rocas Atoll. The significant wave height, which is considered one of the most common parameters in wave spectra validation, was used for this purpose. The ADCPs operated intermittently with a sampling frequency of 2 Hz. Wave characteristics were measured in 2048 bursts (17.1 min) hourly. One ADCP was deployed in the lagoon at a depth of ~2 m, while the other was deployed outside the atoll at a depth of ~16 m (Figure 1). The offshore ADCP was used to assess the agreement between the NWW3 data applied as boundary conditions and the data measured in situ, before reaching the atoll, while the lagoon ADCP was used to assess the quality of the model regarding the wave

transformation through the edge of the atoll and the tidal effect on this process.

The local model reproduced the overall wave conditions well, both offshore and inside the lagoon. The validation results indicated that the bias of the compared stations is 0.106 m (offshore) and 0.027 m (lagoon), and that the RMSE is 0.327 m (offshore) and 0.040 m (lagoon). The correlation coefficient (cc) between modeled (Hmo) and measured (Hme) significant wave height is 0.507 (offshore) and 0.964 (lagoon). The values indicate better model performance in the lagoon. Tidal modulation of waves inside the lagoon has also been resolved by the model. Further details on the model validation can be found in Costa et al. (2019).

RESULTS

Using a validated wave propagation model (as described in Costa et al. 2019), the wave climate inside the lagoon was reconstructed. Results presented below correspond to the analysis of two data series of 35 years each, including one series directly extracted from the global model NWW3 that represents the offshore wave climate and another series reconstructed using the local model MIKE 21 SW that represents the lagoon wave climate. After a visual analysis of the data, the first data year was excluded from both time series due to spurious values. The offshore time series had a total of 102,271 data points with a 3 h interval, whereas the lagoon series had a total of 306,813 data points, considering that the output interval of the local model was 1 h.

Typical conditions

Typical and extreme conditions are shown using classes of wave occurrence values and plotting the results in 2-dimensional histograms (Figure 3). Table 2 outlines the percentage values of the class that represents the mode of the

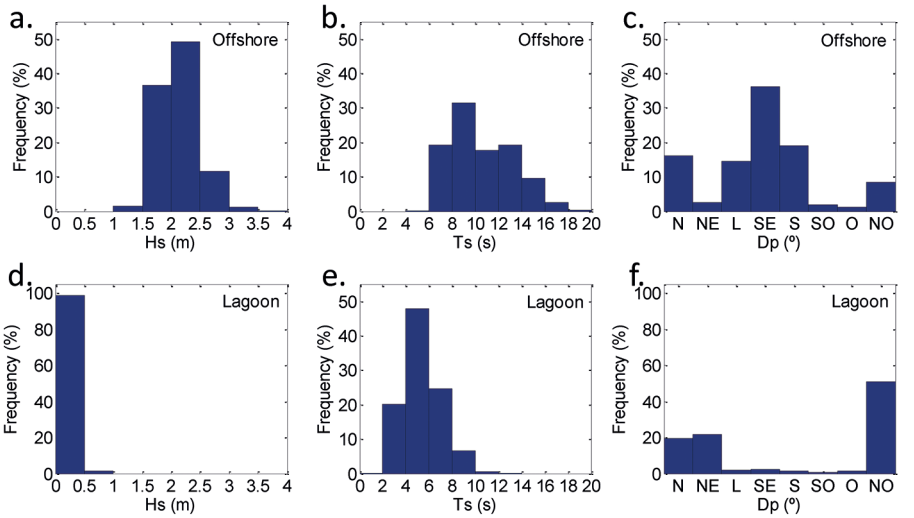

Figure 3. Histograms of (a, d) significant wave height, (b, e) peak period and (c, f) peak direction in the Rocas Atoll lagoon and offshore between 1980 and 2014.

Table 2. Typical and extreme values of significant wave height and peak period for Rocas Atoll.

Pattern	Class	Significant wave height		Peak wave period	
		Range (m)	Percentual (%)	Range (s)	Percentual (%)
Offshore					
Typical	Modal class	2,0 – 2,5	49,2	8,0 – 10,0	31,4
Extreme	Percentil 99%	3,04 – 3,93	1	17,2 – 21,8	1
Lagoon					
Typical	Modal class	0,0 – 0,5	98,6	4,0 – 6,0	47,9
Extreme	Percentil 99%	0,52 – 0,81	1	9,7 – 13,3	1

Tp and Hs distribution. These values are used to characterize the typical wave pattern; the values that occur above the 99% percentile are used to characterize the extreme values.

The significant offshore wave heights range from 1.09 m to 3.93 m, with an average of 2.12 m. Significant wave heights between 2.0 m and 2.5 m were predominant, at 49.2% frequency of occurrence, followed by heights between 1.5 m and 2.0 m, at a frequency of 36.6%. Peak periods had a distribution between 5.2 s and 21.8 s, with a mean of 10.5 s. Periods between 8 s and 10 s occurred in 31.4% of all records and between 6 s and 8 s in 19.3%. Most waves came from the SE (36.1%), followed by the S and N octants, with 19.0% and 16.1% each, respectively, and by the E and NW octants, with 14.4% and 8.5%, respectively. The remaining octants had a frequency of lower than 3% of all occurrences (Figure 3). For the extreme pattern, the 99% percentile covered an Hs range between 3.04 m and 3.93 m and a Tp range from 17.2 s to 21.9 s (Table 2).

The significant lagoon wave heights ranged from 0.01 m to 0.81 m, averaging 0.16 m. Significant heights between 0 m and 0.5 m corresponded to 98.6% of the occurrences in the lagoon, followed by 1.3% for the class between 0.5 and 1.0 m. Peak periods had a distribution between 1.81 s and 13.3 s, with a mean of 5.3 s. Periods between 4 s and 6 s occurred in 47.9% of all records and between 6 s and 8 s in 24.7%. Most waves came from the NW (51.2%), followed by the NE and N octants, with 21.6% and 19.8% each, respectively. The other octants had a frequency lower than 3% (Figure 3). For the extreme pattern in the lagoon, the 99% percentile covered an Hs range between 0.52 m and 0.81 m and a Tp range from 9.7 s to 13.3 s (Table 2).

Directional wave climatologies

Figure 4 shows the directional histograms of the joint distribution of Hs and Tp by directional sector (Dp). The typical offshore SE direction is associated with an Hs and Tp ranging from 2.0 m

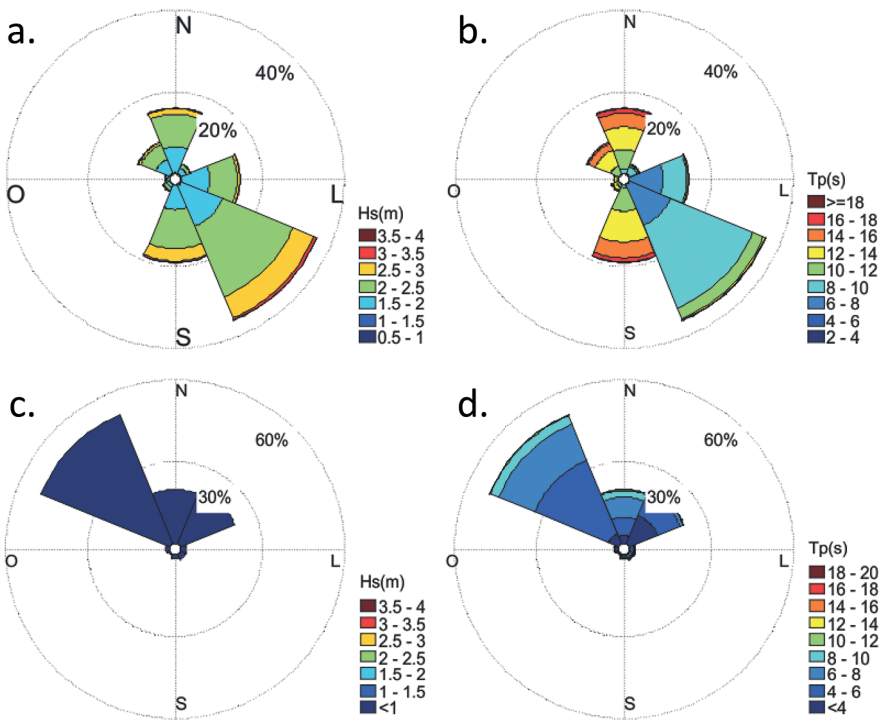

Figure 4. Offshore (a, b) and lagoon (c, d) wave climate of Rocas Atoll. (a, c) Directional histograms of significant wave height (m) and (b, d) directional histogram of the wave peak period (s).

to 2.5 m (51.7%) and from 8 s to 10 s (21.9%), respectively. In this directional sector, the extreme values range from 3.12 m to 3.86 m (1%) and from 12.6 s to 18 s (1%). The S, N, and NW directions are typically associated with waves with longer periods, ranging from 12 s to 14 s (39.8%, 34.3%, and 48.2%, respectively), with heights ranging from 2.0 m to 2.5 m (50.4%, 49.2%, and 46.1%, respectively). The extreme values range from 3.09 m to 3.66 m (1%) and 17.6 s to 20.7 s (1%) for the S sector, from 2.85 m to 3.93 m (1%) and 17.6 s to 21.2 s (1%) for the N sector, and from 2.84 m to 3.50 m (1%) and 17.7 s to 21.8 s (1%) for the NW sector. The E quadrant is associated with waves with shorter periods, ranging from 6 s to 8 s (56.5%), typical Hs from 1.5 m to 2.0 m (47.2%), and extreme values ranging from 2.74 m to 3.14 m (1%) and 11.3 s to 14.4 s (1%).

Throughout the analyzed period, the N, NW, and NE waves with periods longer than 12 s had 23.59% of occurrence, whereas the S, SW, and SE waves with periods longer than 12 s had 23.95%. The remainder (52.46%) consisted of waves with periods shorter than 12 s of various directions, but mainly SE and E.

In the lagoon, all directions were preferentially associated with the Hs class from 0 m to 0.5 m. However, the dominant Tp classes varied with the direction. The class from 4 s to 6 s (57.03%) was predominant for the typical NW direction, whereas the NE and N directions were predominant in the classes from 2 s to 4 s (52.63%) and 6 s to 8 s (37.00%), respectively. The intervals of extreme values of Hs by directional class were 0.26 m to 0.70 m for NW, 0.50 m to 0.81 m for NE, and 0.52 m to 0.72 m for N. The extreme values of Tp ranged from 9.6 s to 12.5 s for NW, 8.8 s to 13.3 s for NE, and 7.8 to 12.2 s for N.

Seasonality

Figures 5 and 6 show the monthly offshore wave climate characteristics, highlighting the seasonality of incident wave fields at Rocas Atoll. Waves from the SE quadrant are present throughout the year, reaching the atoll with greater intensity between July and October. Rocas Atoll experiences the effect of waves from the N and NW quadrant between October to April, with the strongest effect in the percentage of total occurrence of waves derived from this sector in February. Conversely, the waves coming from the S are prominent in May, June, July, August, and September, despite occurring at a low frequency in other months. April is the transition between the N, NW, and S wave

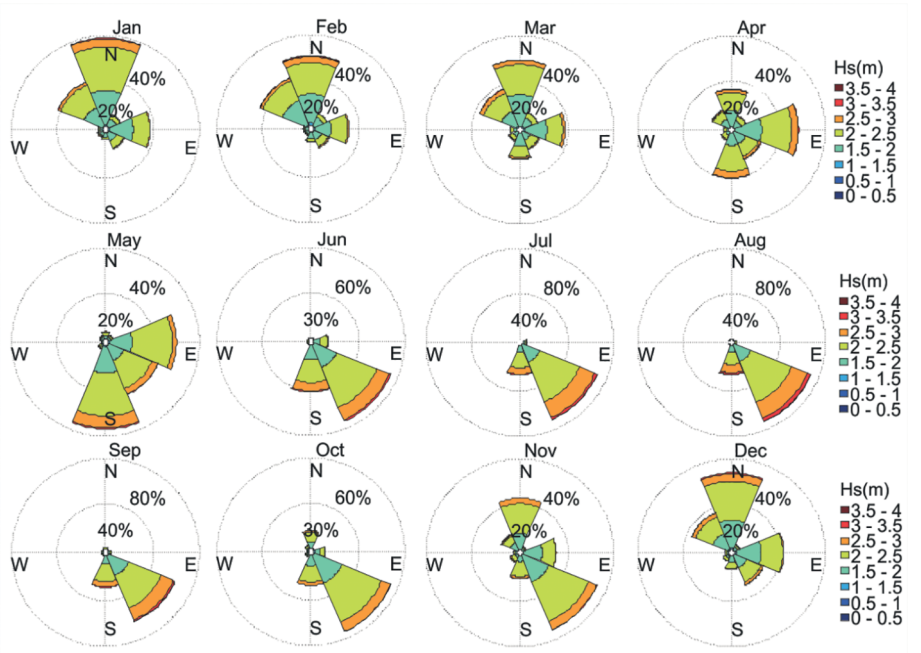

Figure 5. Monthly directional histograms of the significant offshore wave height (Hs).

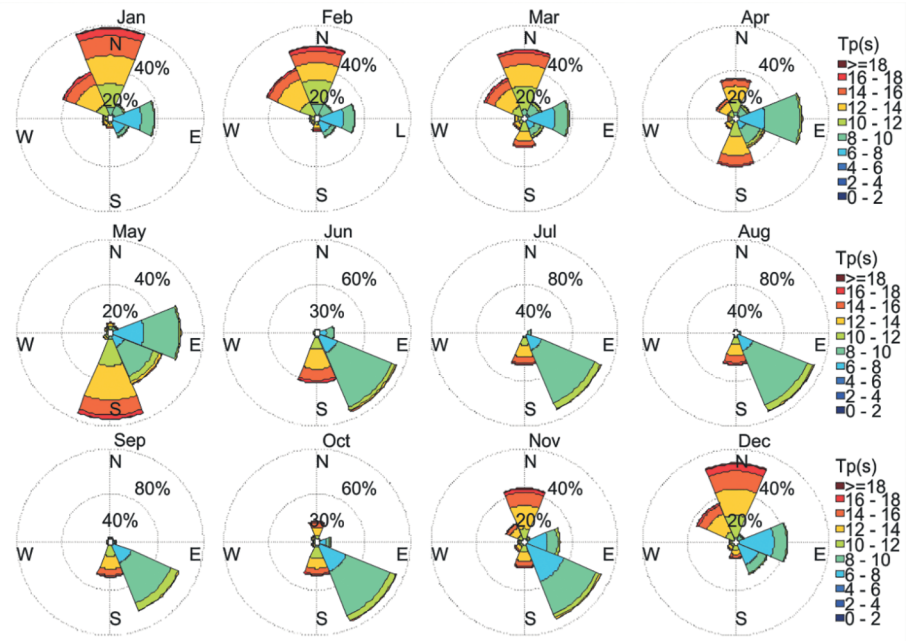

Figure 6. Monthly directional histograms of the offshore peak period (Tp).

fields, displaying the most heterogeneous wave incidence conditions.

In the lagoon, the wave climate is homogeneous throughout the year (Figure 7 and Figure 8). The NW direction is predominant throughout the year, and variation is only observed in the frequency of SE waves, which become more significant from May to November, with the increase in the number of offshore waves from the SE.

Tide and wave climate

As shown in Costa et al. (2019) based on the in situ data, tides have a strong effect on lagoon wave height. The scatter plots demonstrates this relationship based on 35 years of modeled data (Figure 9). As expected, offshore wave conditions have no significant relationship with the tide ($p = 0.6775$). However, the variation in lagoon wave height is positively related to tide ($p < 0.05$, $R^2 = 0.87$), with maximum height limits well defined according to the water level. The waves have a small Hs range (from 0 m to 0.20 m) at low tide (from 0 m to 1 m). The range increases to 0.5 m at intermediary (from 1 m to 2 m) and high (higher than 2 m) tides, and no waves higher than 0.5 m are found at intermediary tide or lower than 0.2 m at high tide. The relation between water level and lagoon wave height defined from 35 years of lagoon modeled data (black line in Figure 9b) was validated by 28 days of measured lagoon wave heights, showing the dependence of lagoon waves on tide. The RMSE from exponential fitted curve and measured wave height is 0.016 m, and the correlation coefficient is 0.95.

Wave extremes

Maximum annual offshore wave heights and periods at Rocas Atoll are summarized in Tables S1 and S2 (Supplementary Material). The maximum offshore wave heights occur mainly in August and are generated by events that occur in the Southern Hemisphere (S, SW, or SE wave directions). They are accompanied by peak periods averaging 12 s. However, maximum wave height values derived from the Northern Hemisphere (N, NW, or NE wave directions) are associated with higher peak period values (mean of 16.3 s) that may represent more energetic conditions. These events from the Northern Hemisphere stand out as annual maxima, occurring only 5 times in 35 years. In turn, the occurrence of peak period annual maxima has a more homogeneous distribution in relation to the hemisphere of origin, though most (57% of occurrences) are from the

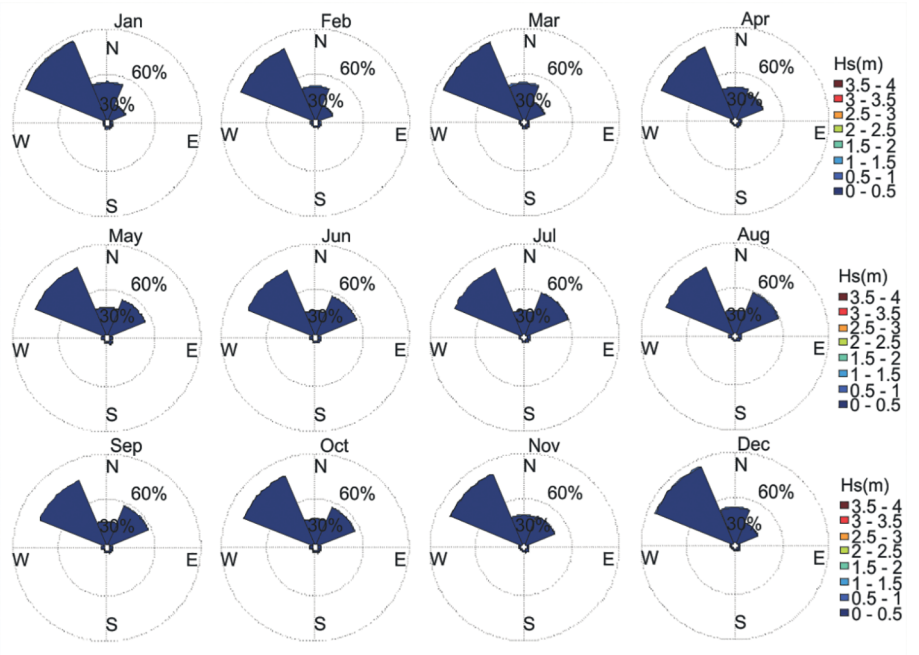

Figure 7. Monthly directional histograms of the significant lagoon wave height (Hs).

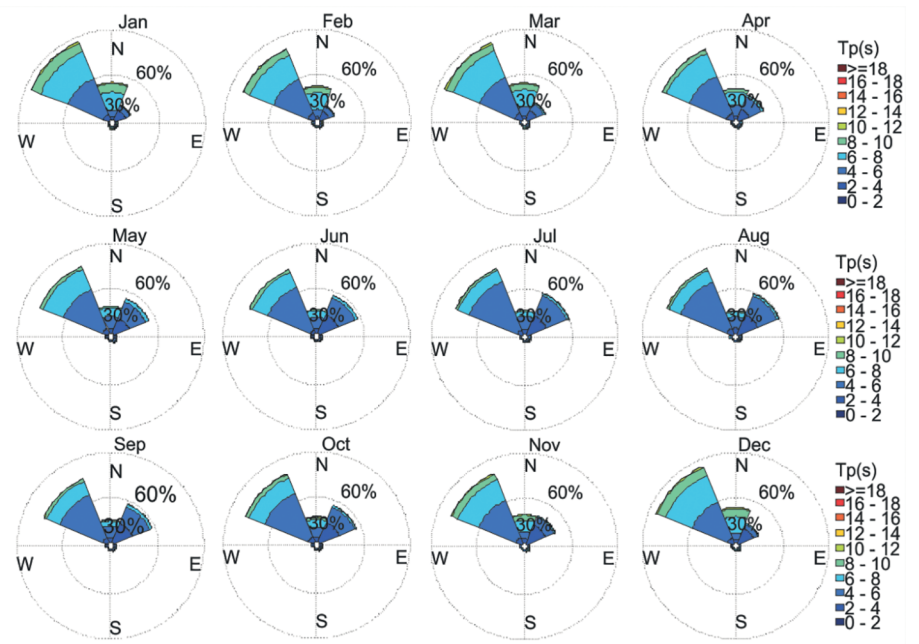

Figure 8. Monthly directional histograms of the lagoon peak period (Tp).

Northern Hemisphere and occur predominantly in December. The heights associated with the maximum periods do not exceed 3 m, with a mean of 2 m. The random tide values associated with the annual maxima are observed, highlighting the lack of relationship between the two variables.

The maximum annual lagoon wave heights occurred concurrently with the spring high tides. This is expected since higher waves may only propagate into the lagoon during high tides, demonstrating the tidal dependence of extreme wave conditions inside the atoll. The annual maxima of both

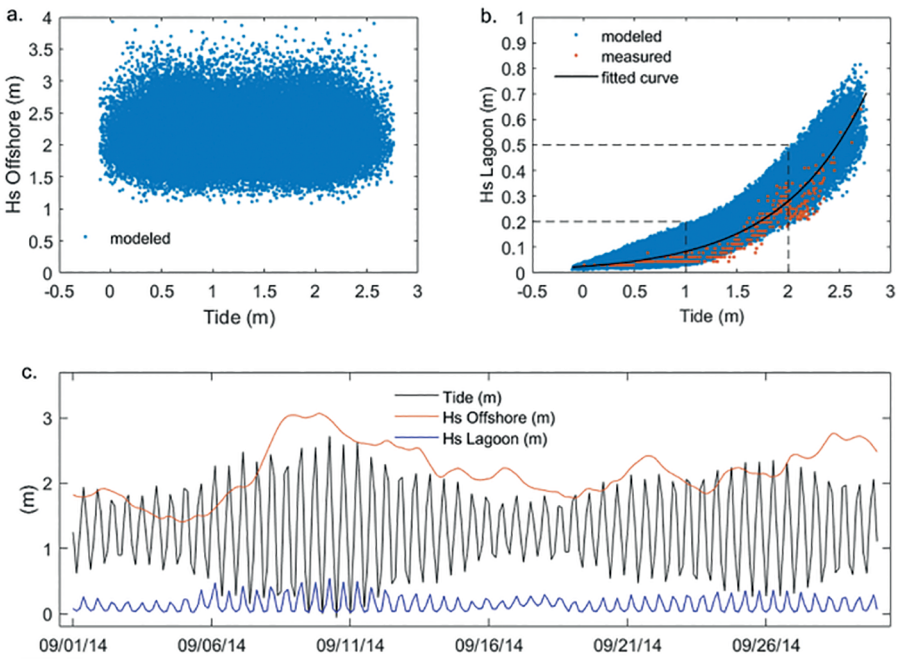

Figure 9. (a) Scatter plot of offshore modeled wave and tide height and (b) lagoon modeled and measured wave and tide height. The black line represents the exponential fitted curve for 35 years of modeled wave height dataset. (c) Example of time series during September 2014 demonstrating the tidal oscillation and offshore and lagoon modeled wave heights.

Hs and Tp were preferentially northerly. However, nearly half the annual maxima of Hs (45%) were southerly.

The Hs and Tp maxima are not necessarily associated, as shown in Tables S1 and S2 (Supplementary material). The analysis of the joint occurrence of Hs and Tp by the wave power parameter ranged from 4.54 kW/m to 142.53 kW/m, averaging 27.98 kW/m offshore. The "Moderate" intensity class was the most common in the region. Conversely, the lagoon wave power was restricted to 0 - 4.46 kW/m, averaging 0.14 kW/m, with all events falling within the "Calm" class. Offshore, the class of extreme wave power events accounted for 5.96% of all occurrences (Figure 10).

The analysis of the frequency of classes by offshore direction, demonstrates that most extreme events reached the atoll from the Southern and Northern Hemispheres (Figure 11). Events stronger than 80 kW/m had a similar N and S distribution (3.19% from N and 3.14% from S), and events stronger than 90 kW/m were predominantly northerly (1.32% from N and 1.04% from S).

Return periods

To establish the mean return periods of extreme events for Rocas Atoll, the Generalized Extreme Value (GEV) model was used to extrapolate the extreme values beyond the range available in the original series. The GEV model was applied to the series of offshore and lagoon annual maxima (of Hs, Tp, and P), using the maximum likelihood estimation (MLE) method to estimate the model parameters. No estimates beyond 100 years were used because the forecast uncertainty increases with the analysis period, and estimates not exceeding twice the length of the time series used (35 years in this case) are recommended. Figure 12 contains the GEV fit-quality plots for the series of annual maxima of wave parameters.

The maximum event observed in the 35-year series, which occurred in February 1982 (P = 142 kW/m), has a return period of approximately 38 years (Figure 13). This event occurred together with a spring tide with a height of 2.57 m, resulting in conditions of 3.18 kW/m P and 0.75 m and 9.9 s Hs and Tp, respectively, in the lagoon. Conversely,

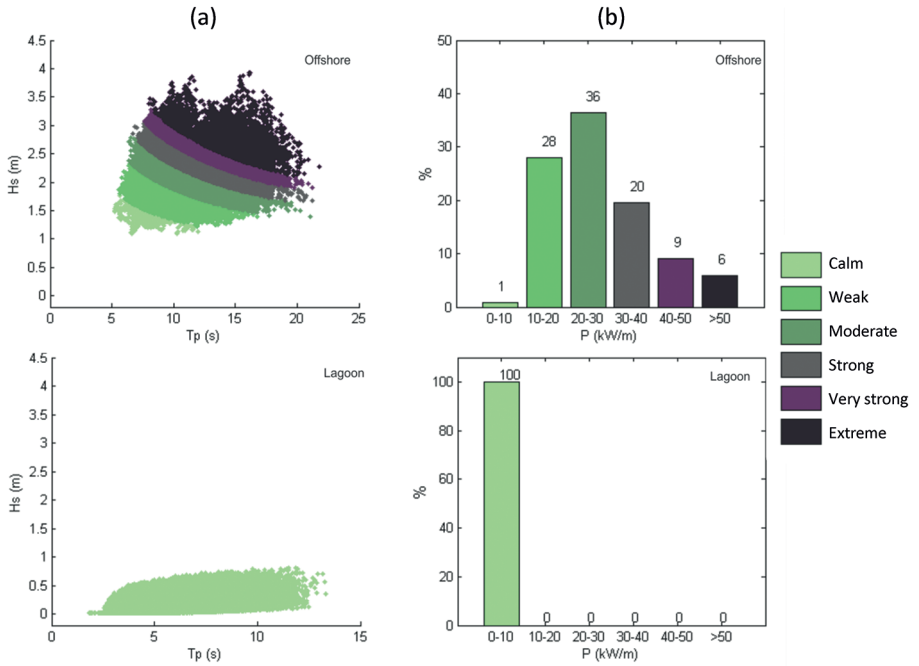

Figure 10. (a) Scatter plots of combined occurrences of significant wave height (Hs) and peak period (Tp) and (b) histograms of wave power (P) during the 35-year interval, offshore and in the lagoon. The color scale represents the wave intensity classes. The values above each bar are the rounded percentage of occurrence values.

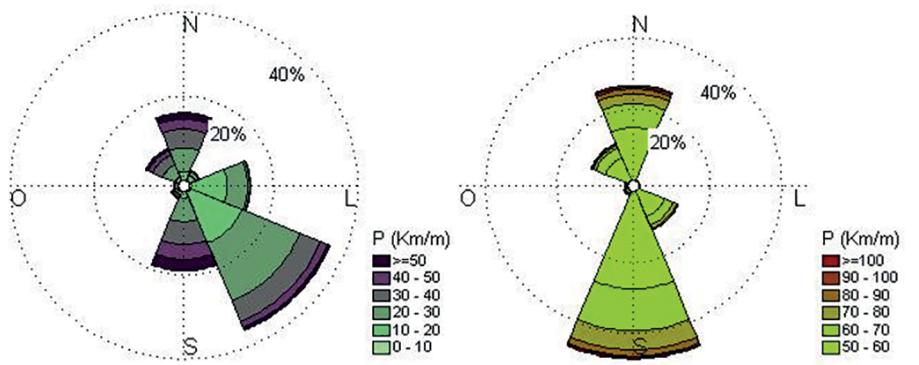

Figure 11. Directional histograms of wave power (P) for the (a) total dataset and (b) the class of extremes only (P ≥ 50 kW/m).

the largest wave event recorded in the lagoon occurred in March 1981 during a spring tide of 2.65 m, with waves of 0.81 m and 11.8 s, resulting in 4.46 kW/m P.

Offshore events with Hs higher than 3.75 m or Tp longer than 21.3 s and P greater than 118.31 kW/m had return periods longer than 10 years and a 10% annual probability of exceedance. Table 3 outlines the return periods of 2, 5, 10, 25, 50, and 100 of Hs, Tp, and P magnitudes. The probability of exceedance of each of these periods at any year is 50%, 20%, 10%, 4%, 2%, and 1%, respectively.

Furthermore, Table 4 presents the highest wave power values and their associated direction. Offshore extreme events (> 50 kW/m) showed annual recurrence with a frequency of five per year, originating in both Northern and the Southern Hemispheres. However, events with a magnitude higher than 95 kW/m occurred on average every three years, and in four of the twelve years, events

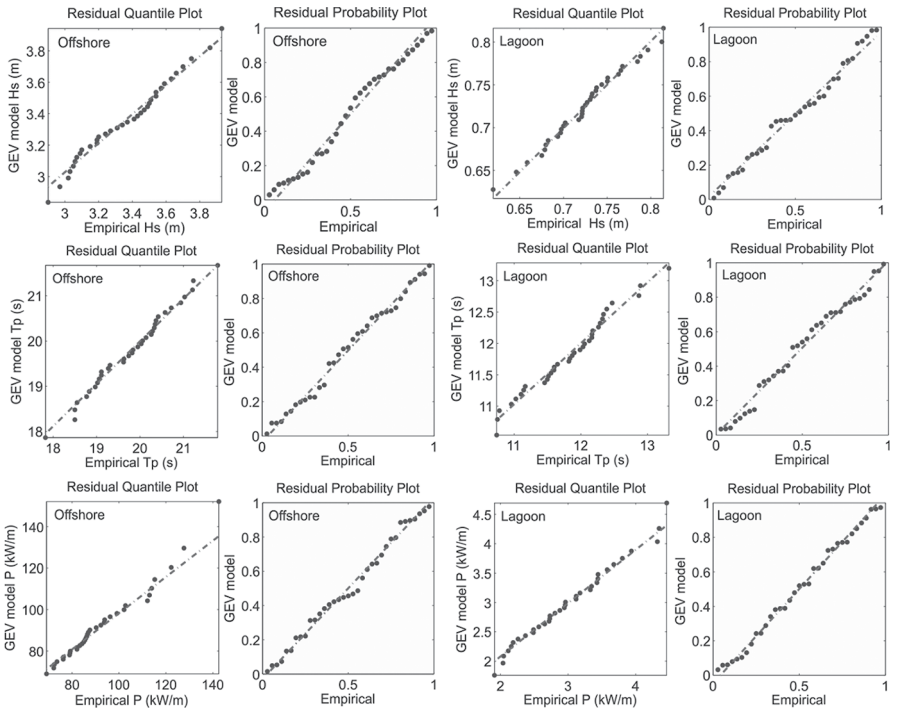

Figure 12. Probability and quantile plots corresponding to the 35-year maximum values fit to the Generalized Extreme Value (GEV) distribution.

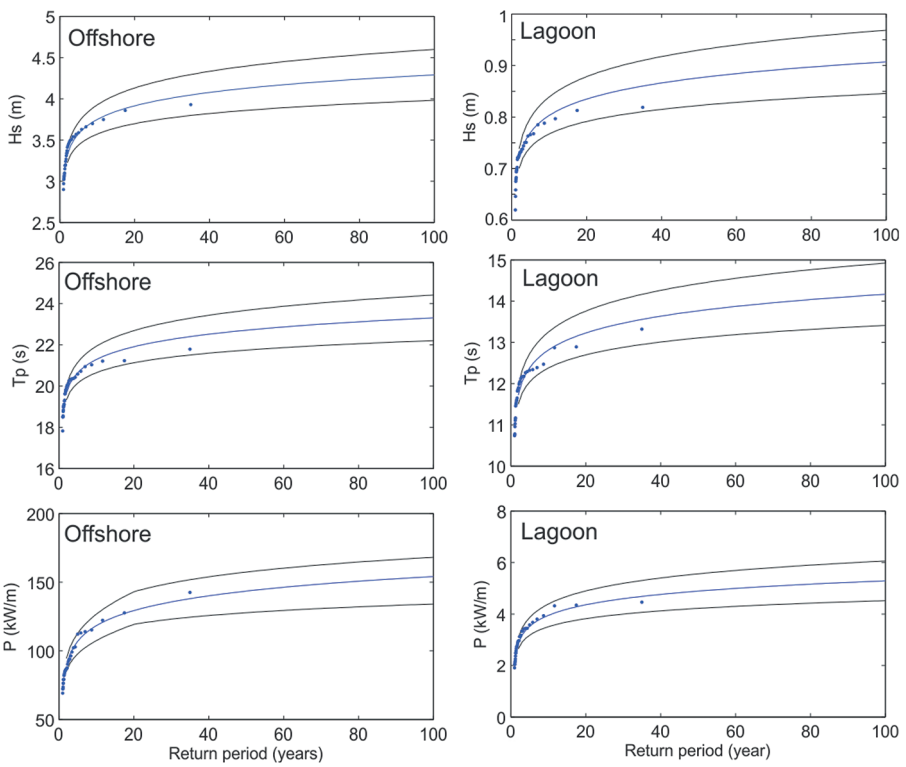

Figure 13. Return period of wave extremes estimated using the GEV distribution based on the 35-year time series of Hs, Tp, and P for offshore and Hs, Tp, and P for the lagoon.

Table 3. Estimates of wave extremes for the various return periods, based on the 35-year offshore time series for Rocas Atoll.

Return period (years)	Offshore			Lagoon		
	Hs (m)	Tp (s)	P (kW/m)	Hs (m)	Tp (s)	P (kW/m)
2	3.32	19.66	89.63	0.72	11.73	2.87
5	3.56	20.64	106.88	0.77	12.38	3.52
10	3.75	21.29	118.31	0.80	12.81	3.95
25	3.97	22.1	132.74	0.85	13.36	4.49
50	4.13	22.71	147.44	0.88	13.76	4.89
100	4.29	23.31	154.07	0.91	14.12	5.23

Table 4. Most energetic wave events recorded offshore of Rocas Atoll in the last 35 years (1980-2014), using the occurrence of 1% of the total number of events of the classes of extremes (> 50 kW/m) and considering the peak of each event.

1% of P (kW/m) maximum values									
Offshore					Lagoon				
Year	Month	P (kW/m)	Tide (m)	Direction	Year	Month	P (kW/m)	Tide (m)	Direction
1982	2	142.53	2.57	N	1981	3	4.46	2.65	NE
2011	8	127.65	2.13	S	2001	2	4.35	2.70	NE
1983	12	122.24	1.94	N	1999	10	4.32	2.63	NE
2013	8	115.22	2.10	S	1987	2	3.94	2.65	NE
2014	5	113.93	2.31	S	1991	1	3.80	2.59	NE
1999	8	112.98	2.31	S	1985	2	3.67	2.54	NE
1985	2	112.12	2.54	NO	2006	3	3.58	2.71	NE
1999	1	106.06	2.52	N	2005	10	3.44	2.51	NE
2007	8	102.74	2.31	SE	1992	1	3.44	2.68	NE
1985	12	102.35	1.91	N	1999	1	3.43	2.52	NE
1996	8	102.16	1.97	S	1988	2	3.43	2.76	NE
1981	5	99.11	2.14	S	1995	1	3.35	2.64	NE
1981	3	98.01	2.65	NO	1994	2	3.33	2.65	NE
1996	9	97.24	1.81	SE	1982	2	3.18	2.57	NE
2009	12	96.23	2.04	N	1990	2	3.12	2.58	NE

of this magnitude are observed twice in the same year. Another observation concerns the distribution according to direction. In the last 35 years, extreme events from the N occurred mainly in the 1980s, at approximately 1-year intervals between 1981 and 1985, whereas the events from the S occurred mainly in the last decade, at approximately 2-year intervals between 2007 and 2014.

The maximum events in the lagoon did not necessarily occur in the same order of offshore events. The occurrence of these events was related to a spring tide with at least 2.50 m. These events occurred from October to March (preferentially in February), months that correspond to the predominance of incidence of events originated in the Northern Hemisphere (Figure 5 and Figure 6). Regarding direction, the classes outlined in Table 4 reflect the direction of wave entry into the lagoon, which is not necessarily its offshore direction.

DISCUSSION

Offshore wave climate

The results of the analysis of typical and seasonal conditions display the wide directional variability of wave events that characterize the offshore

wave climate of Rocas Atoll. Being located at low latitudes, this region is exposed to a regime of sea surface waves formed as much by waves generated by local winds (wind waves) as by waves generated by distant winds (swell) in both hemispheres. Local winds acting in the south equatorial region, where Rocas Atoll is located, are the southeast trade winds (Innocentini et al. 2005), which are responsible for the formation of wind waves. Conversely, swells are formed by distant weather events, including extratropical cyclones in the Northern and Southern Hemispheres and East African atmospheric waves (Innocentini et al. 2005).

The direction of wave incidence at Rocas is subject to annual seasonality, which is affected by the wind regimes at synoptic scale. Waves reaching the Rocas Atoll may be categorized into three main groups according to their period characteristics and associated direction:

Group 1: SE octant waves, present in the atoll during the entire year, are wind waves, formed by local wave fields forced by southeast trade winds. These winds accompany semi-permanent anticyclones of the North and South Atlantic and experience a southern shift according to the annual solar cycle, intensifying from July to October (Innocentini et al. 2005). Offshore winds of up to 14 m/s may be observed during this period. E octant waves are also wind sea waves. They are lower energy than southeasterly waves and are most likely associated with periods of shift to the south of the Intertropical Convergence Zone and the local weakening of trade winds.

Group 2: The waves derived from the N and NW that reach the atoll region are swell waves, generated in wind fields acting in the Northern Hemisphere that intensify during the winter of this hemisphere and have the ability to propagate throughout much of the Atlantic Ocean basin. Thus, these waves reflect the sea agitation generated by surface winds that accompany extratropical cyclones, which are very intense during this season off the northeastern sector of the North Atlantic (Innocentini et al. 2005).

Group 3: The S and SW octant waves are swell waves and reach Rocas Atoll with greater intensity during the Southern Hemisphere winter months. They are mainly generated at latitudes higher than 40° S and propagate northerly and northeasterly, losing energy during this process. On the south coast of Brazil, waves higher than 5 m may move to the coastal zone (Pianca et al. 2010). Conversely, in the Rocas Atoll region, waves with this value are not observed, and waves higher than 3 m derived from the Southern Hemisphere are rare.

The three main groups of waves may occur simultaneously throughout the year. In particular, Group 1 occurs almost year round, always overlapping with Groups 2 and/or 3, given the permanent southeasterly trade winds in the region. Conversely, these last two groups tend to switch seasonally, depending on the seasonal variation in wind intensity at high latitudes and the ratio of incidence throughout Rocas. The swell from both hemispheres exhibits similar frequencies.

The Hs values exhibited low variability and mild conditions compared to the wave climate of high-latitude regions, despite the high directional variability of incident waves at Rocas Atoll (Young 1999). Such characteristics are also the result of the location of the atoll in the equatorial region. The zonal (latitudinal) distribution of Hs in the globe shows that the highest wave conditions are observed at higher latitudes. This is particularly evident in the Southern Ocean, where intense wave conditions are observed throughout the year, despite peaking during winter in the Southern Hemisphere (July-August) (Young 1999). Furthermore, the west coasts of continents receive more energy from swell propagation originating at high latitudes because of the propagation towards the northeast along the great circle path (Young 1999). Rocas, which is near the east coast of South America, receives less swell energy compared to the equatorial region near the coast of Africa.

Lastly, its position slightly south of the equator allows the atoll to remain outside the path of Atlantic tropical cyclones, which are formed in latitudes between 5° and 30° N and typically move westward (Emanuel 2003; Colbert and Soden 2012). These three factors regarding atoll location result in overall mild wave conditions throughout the year.

Lagoon wave climate

The results show that offshore waves are significantly changed when propagating into the lagoon, resulting in a different and far more homogeneous inner wave climate. The atoll morphology and tides, in particular, play key roles in controlling the directional and energy characteristics of the wave climate in the lagoon.

The directional variability in the lagoon is mainly restricted to the N, NW, and NE directions, which match the direction of the main reef passage (Barretão), indicating that waves penetrate the lagoon mainly through this passage. In particular, the typical wave propagation direction in the lagoon is opposite the typical offshore direction of dominant waves forced by local wind (Group 1, mentioned above), showing the refraction effect of offshore waves from various directions in the vicinity of the atoll rim and penetration through the channel.

Although Barretão is located in the zone protected from constant SE waves, results suggest that this is the most energetic zone of wave propagation to the lagoon, due to wave refraction. Spatial differences in the type and magnitude of wave energy are generally found on atolls due to differences in the reef flat elevation (Kench 1998a), and more energetic waves should be found in the vicinity of reef passages (Aucan et al. 2012). These studies also highlight the dependence of the wave lagoon characteristics on atoll morphology.

In terms of wave energy, the significant wave height in the Rocas Atoll lagoon is approximately 60% smaller than offshore and typically does not exceed 0.8 m, even during the incidence of energetic ocean swells (for example, offshore Hs of 3.5 m). Reduction in wave height occurs through energy dissipation when the wave interacts with the reef structure (Kench et al. 2006). In addition to attenuation by depth-limited breaking, waves propagating across the reef flat or narrow reef channels can dissipate significant amounts of energy due to bottom friction (Lowe 2005; Lowe et al. 2009a). Thus, the reef rim serves as a low-pass wave height filter by filtering out waves with heights larger than the depth-limited maximum (Lowe 2005). In combination with bottom friction, it imposes major constraints on ocean swell, leading to dramatic transformations in wave characteristics and the consequent rapid attenuation of wave energy (Kench and Brander 2006a).

Results for Rocas show a clear separation between lagoon wave height values according to tide level. Wave height variability, despite having a smaller range than the offshore waves, occurs in shorter and more regular periods of time. The waves vary in a 6-h scale, according to the high and low tide level at the time. This strong modulation is the result of the water level in the reef edge and in the Barretão passage. During low tides, the reef rim is emerged and the lagoon water is connected only by the reef passage. During intermediary and high tides, waves break on the reef rim and propagate into the atoll, refracting on the shallow reef rim. The topography of the Rocas Atoll rim is irregular, with the highest parts in the windward region and the lowest parts in the leeward region, as shown in Costa et al. (2017a, 2019). Thus, the wave may penetrate with more energy through the parts with a higher water level on the edge because of the refraction process. Furthermore, at high tide, the water level in Barretão passage increases, which reduces the energy dissipation due to bottom friction during channel wave propagation.

Wave energy that is transmitted across the reef crest propagates into the lagoon and reaches the Rocas reef islands (Farol and Cemitério islands). The residual energy that follows wave breaking and energy dissipation becomes the incident energy that is instrumental in causing island beach change (Kench et al. 2006). However, the tidal modulation of wave energy limits the amount of time that geomorphic work can occur on reefs (Kench et al. 2006). Direct sediment remobilization by waves can only occur at high tide, when more energetic waves penetrate the lagoon and water covers the beach side boundaries of Farol and Cemitério islands. At low tide, waves remain virtually constant at a height of 0.2 m, regardless of offshore conditions; the vicinity of the island is exposed, and the submerged area of the lagoon is reduced. The effect of waves is therefore limited both in area and magnitude throughout a tidal cycle.

However, even when the wave energy level in the lagoon is greatly reduced because of tide level, wave breaking and wave set-up result in water volumes being continuously pumped into the atoll, which is an important hydrodynamic control inside the atoll (Costa et al. 2017b). Wave pumping is one of the main drivers of mean wave-driven currents across reef systems and controls ocean-lagoon flow in atolls (Callaghan et al. 2006; Hench et al. 2008; Lowe et al. 2009b; Costa et al. 2017a).

Extreme events

As noted above, Rocas has a mild wave climate throughout the year because of its geographic position on the western edge of the South Atlantic, near the equator. The results show that extreme wave events are mainly related to the energy dissipation process of swell (Groups 2 and 3) incidents on the shallow waters of the atoll, and that the tide plays a key role in selecting which offshore energetic events may reach the interior of the atoll.

Due to the tidal effect on the dissipation process, extreme offshore conditions do not necessarily cause extreme conditions in the lagoon. Extreme events in Pacific and Indian atolls, located outside the tropical cyclone belt, have been associated with the dissipation of wind waves generated by distant extra-tropical cyclones (swell), especially if they occur during high tides (Hoeke et al. 2013). However, because Rocas is a mesotidal atoll, both high tides and high spring tides are required to generate extreme events inside the lagoon. This is mainly observed in extreme offshore events that occur in combination with neap high tides and do not result in extreme events in the lagoon. With spring and neap tidal cycles alternating every ~15 days, the variation between high tides may reach 1 m, generating considerable variations in water level and height in relation to the atoll rim, which may significantly limit energy transmission into the atoll.

High-energy waves breaking on the reef rim can cause extreme sea levels and currents that, during high tides, may lead to inundation (Aucan et al. 2012) and/or great morphological changes in the reefs and reef islands (Smithers and Hoeke 2014). Inundation of near-equatorial (between 5° N and 5° S) low lying islands, severe in some cases, has been documented throughout the Pacific Ocean and in the Indian Ocean by swell-driven sea level anomalies that add to high tides (Hoeke et al. 2013). In Rocas, flood events have been observed periodically. However, no recorded data on the severity and extent of these floods exists. Extreme events coinciding with spring high tides may be the main causes of such floods. Furthermore, high wave set-up is generally accompanied by high wave run-up, energetic near-shore currents, and possibly complex nonlinear effects such as infragravity waves, all of which may greatly exacerbate inundation and morphological changes in reef islands (Hoeke et al. 2013).

The incoming swell direction may also affect the energy distribution throughout the atoll (Kench et al. 2006) and cause large reversals in sediment flux and significant changes in atoll island shorelines (Kench and Brander 2006b). In Rocas, results do not indicate a predominant direction of extreme events, that is, the swell generated both in the Northern and Southern Hemispheres contributed equally to the occurrence of potential extreme events on the atoll. However, the more energetic conditions of the lagoon are mainly related to the northern swells combined with spring tides. This finding may be explained by the atoll morphology. Because the main passage (Barretão) faces north, waves approaching from this direction may propagate to the lagoon with less dissipation. Conversely, waves generated in the Southern Hemisphere experience great energy dissipation in the windward rim reach the channel after refracting.

Extreme events from the north may also impact the reef islands more directly because of their position in the northwestern part of the atoll, only a few meters from the reef edge. Furthermore, the reef crest on this side is lower than the crest on the exposed side (Costa et al. 2019). Thus, at high tide the water column is increased on this side, allowing more wave energy transmission into the lagoon. Conversely, extreme events that directly affect the southeastern edge of the atoll (windward) may contribute to the detachment and remobilization of coarse fractions of the reef and

the availability of sediments (e.g. Gourlay 1988). Although the occurrence of such extreme events presents longer recurrence ranges and short durations (only few hours), it may initiate changes that last several years until a new stable situation develops (Gourlay 1988).

CONCLUSIONS

Based on modelled and observed wave data, for the first time we present the wave climate in and around the Rocas atoll. The offshore wave climate that reaches the region presents a wide directional variability, with sea and swell waves reaching the region from both hemispheres. The direction of wave incidence at Rocas is subject to annual seasonality, which is affected by the wind regimes at synoptic scale. Once reaching the atoll, the local morphology, combined with tides, play an important role in wave transformation processes and consequently on how the waves propagate into the lagoon. Directional variability in the lagoon is mainly restricted to the N, NW, and NE directions, which match the direction of the main reef passage, indicating that waves penetrate the lagoon mainly through this passage. In terms of wave energy, the significant wave height in the Rocas Atoll lagoon is approximately 60% smaller than offshore and typically does not exceed 0.8 m, even during the incidence of energetic ocean swells. Energetic wave conditions inside the lagoon are mainly related to the northern swell combined with spring tide. At low tide, the waves remain virtually constant at a height of 0.2 m, regardless of offshore conditions; the vicinity of the islands is exposed, and the submerged area of the lagoon is reduced. Tides and morphology are the main controls on the Rocas Atoll wave climate, subject to a mesotidal regime and with complex rim morphology.

ACKNOWLEDGMENTS

This study was funded by CNPq through the project “Processos induzidos por ondas e mares no Atol das Rocas: implicações geomorfologicas e projecoes futuras” (CNPq 486572/2012-9), by the INCT Ambientes Tropicais Marinhos (CNPq/MCTI), CAPES (001) and by FAPESP (Fundacao de Apoio a Pesquisa do Estado de Sao Paulo, Brazil N° 2011/22661-3). We are grateful to the ICMBio (Instituto Chico Mendes de Conservação da Biodiversidade), especially to Maurizélia Brito, the manager of the marine protected area of Rocas Atoll (REBIO Atol das Rocas/ICMBio/MMA), who granted permits and provided all the needed support to our expeditions. E.S. is a CNPq research fellow. Authors are also grateful to the three anonymous reviewers and editors for providing useful comments that improved our manuscript.

AUTHOR CONTRIBUTIONS

M.B.C.: conceptualization; methodology; software; formal analysis; investigation; resources; data curation; writing—original draft; writing—review and editing; project administration.

E.S.: conceptualization; methodology; resources; writing—original draft; writing—review and editing; supervision; project administration; funding acquisition.

REFERENCES

ABELSON, A. & DENNY, M. 1997. Settlement of marine organisms in flow. *Annual Review of Ecology and Systematics*, 28, 317-339.

AMORES, A., MARCOS, M., PEDREROS, R., LE COZANNET, G., LECACHEUX, S., ROHMER, J., HINKEL, J., GUSSMANN, G., VAN DER POL, T., SHAREEF, A. & KHALEEL, Z. 2021. Coastal flooding in the Maldives induced by mean sea-level rise and wind-waves: from global to local coastal modelling. *Frontiers in Marine Science,* 8, 665672, DOI: https://doi.org/10.3389/fmars.2021.665672

ATKINSON, M., SMITH, S. V. & STROUP, E. D. 1981. Circulation in Enewetak Atoll lagoon. *Limnology and Oceanography,* 26(6), 1074-1083.

AUCAN, J., HOEKE, R. K. & MERRIFIELD, M. A. 2012. Wave-driven sea level anomalies at the Midway tide gauge as an index of North Pacific storminess over the past 60 years. *Geophysical Research Letters*, 39(17), 1-6, DOI: https://doi.org/10.1029/2012GL052993

BEETHAM, E. P. & KENCH, P. S. 2014. Wave energy gradients and shoreline change on Vabbinfaru platform, Maldives. *Geomorphology*, 209, 98-110, DOI: https://doi.org/10.1016/j.geomorph.2013.11.029

BEETHAM, E., KENCH, P. S., O’CALLAGHAN, J. & POPINET, S. 2016. Wave transformation and shoreline water level on Funafuti Atoll, Tuvalu. *Journal of Geophysical Research: Oceans*, 121(1), 311-326, DOI: https://doi.org/10.1002/2015JC011246

BDC (Banco de Dados Climatológicos do Comando da Aeronáutica). 2015. *Dados para a estação SNFN entre o período de 2006 a 2014* [online]. Brasília: BDC. Available at: http://www.icea.gov.br/climatologia/index.html [Accessed: 2015 May 10].

BLACK, K. P. 1993. The relative importance of local retention and inter-reef dispersal of neutrally buoyant material on coral reefs. *Coral Reefs*, 12, 43-53, DOI: https://doi.org/10.1007/BF00303783

BRANDER, R. W., KENCH, P. S. & HART, D. 2004. Spatial and temporal variations in wave characteristics across a reef platform, Warraber Island, Torres Strait, Australia. *Marine Geology*, 207(1-4), 169-184, DOI: https://doi.org/10.1016/j.margeo.2004.03.014

CALLAGHAN, D. P., NIELSEN, P., CARTWRIGHT, N., GOURLAY, M. R. & BALDOCK, T. E. 2006. Atoll lagoon flushing forced by waves. *Coastal Engineering*, 53(8), 691-704, DOI: https://doi.org/10.1016/j.coastaleng.2006.02.006

CAMUS, P., MENDEZ, F. J. & MEDINA, R. 2011. A hybrid efficient method to downscale wave climate to coastal areas. *Coastal Engineering*, 58(9), 851-862, DOI: https://doi.org/10.1016/j.coastaleng.2011.05.007

CAMUS, P., MENDEZ, F. J., MEDINA, R., TOMAS, A. & IZAGUIRRE, C. 2013. High resolution downscaled ocean waves (DOW) reanalysis in coastal areas. *Coastal Engineering,* 72, 56-68, DOI: https://doi.org/10.1016/j.coastaleng.2012.09.002

CHARLES, E., IDIER, D., DELECLUSE, P., DÉQUÉ, M. & LE COZANNET, G. 2012. Climate change impact on waves in the bay of Biscay, France. *Ocean Dynamics*, 62, 831-848, DOI: https://doi.org/10.1007/s10236-012-0534-8

CHARLES, E., IDIER, D., THIÉBOT, J., LE COZANNET, G., PEDREROS, R., ARDHUIN, F. & PLANTON, S. 2012. Present wave climate in the bay of biscay: Spatiotemporal variability and trends from 1958 to 2001. *Journal of Climate*, 25(6), 2020-2039, DOI: https://doi.org/10.1175/JCLI-D-11-00086.1

CHINI, N., STANSBY, P., LEAKE, J., WOLF, J., ROBERTS-JONES, J. & LOWE, J. 2010. The impact of sea level rise and climate change on inshore wave climate: A case study for East Anglia (UK). *Coastal Engineering*, 57(11-12), 973-984, DOI: https://doi.org/10.1016/j.coastaleng.2010.05.009

COLBERT, A. J. & SODEN, B. J. 2012. Climatological variations in North Atlantic tropical cyclone tracks. *Journal of Climate*, 25(2), 657-673, DOI: https://doi.org/10.1175/JCLI-D-11-00034.1

COSTA, M. B., MACEDO, E. C. & SIEGLE, E. 2017. Planimetric and volumetric changes of reef islands in response to wave conditions. *Earth Surface Processses and Landforms*, 42(15), 2663-2678, DOI: https://doi.org/10.1002/esp.4215

COSTA, M. B., MACEDO, E. C. & SIEGLE, E. 2019. Wave refraction and reef island stability under rising sea level. *Global and Planetary Change*, 172, 256-267, DOI: https://doi.org/10.1016/j.gloplacha.2018.10.015

COSTA, M. B., MACEDO, E. C., VALLE-LEVINSON, A. & SIEGLE, E. 2017. Wave and tidal flushing in a near-equatorial mesotidal atoll. *Coral Reefs*, DOI: https://doi.org/10.1007/s00338-016-1525-x

DUMAS, F., LE GENDRE, R., THOMAS, Y. & ANDRÉFOUËT, S. 2012. Tidal flushing and wind driven circulation of Ahe atoll lagoon (Tuamotu Archipelago , French Polynesia) from in situ observations and numerical modelling. *Marine Pollution Bulletin*, 65(10-12), 425-440, DOI: https://doi.org/10.1016/j.marpolbul.2012.05.041

EMANUEL, K. 2003. Tropical cylones. *Annual Review of Earth and Planetary Sciences*, 31, 75-104, DOI: https://doi.org/10.1146/annurev.earth.31.100901.141259

FRITH, C. A. & MASON, L. B. 1986. Modelling wind driven circulation One Tree Reef, Southern Great Barrier Reef. *Coral Reefs*, 4, 201-211.

GOURLAY, M. R. 1988. Coral cays: products of wave action and geological processes in a biogenic environment. *In: Proceedings of the 6th International Coral Reef Symposium (ICRS).* Townsville, Australia. Townsville: ICRS, v. 2, pp. 6-11.

HAMNER, W. & WOLANSKI, E. 1988. Hydrodynamic forcing functions and biological processes on coral reefs: a status review. *In: Proceedings of the 6th International Coral Reef Symposium (ICRS).* Townsville, Australia. Townsville: ICRS, v. 1, pp. 103-113.

HEARN, C., ATKINSON, M. & FALTER, J. 2001. A physical derivation of nutrient-uptake rates in coral reefs: effects of roughness and waves. *Coral Reefs*, 20, 347-356, DOI: https://doi.org/10.1007/s00338-001-0185-6

HENCH, J. L., LEICHTER, J. J. & MONISMITH, S. G. 2008. Episodic circulation and exchange in a wave-driven coral reef and lagoon system. *Limnology and Oceanography*, 53(6), 2681-2694, DOI: https://doi.org/10.4319/lo.2008.53.6.2681

HOEKE, R. K., MCINNES, K. L., KRUGER, J., MCNAUGHT, R. J., HUNTER, J. R. & SMITHERS, S. G. 2013. Widespread inundation of Pacific islands triggered by distant-source wind-waves. *Global and Planetary Change*, 108, 128-138, DOI: https://doi.org/10.1016/j.gloplacha.2013.06.006

HOEKE, R. K., STORLAZZI, C. & RIDD, P. 2011. Hydrodynamics of a bathymetrically complex fringing coral reef embayment: wave climate, in situ observations, and wave prediction. *Journal of Geophysical Research: Oceans*, 116(C4), C04018, DOI: https://doi.org/10.1029/2010JC006170

HOLTHUIJSEN, L. H., BOOIJ, N. & HERBERS, T. H. C. 1989. A prediction model for stationary, short-crested waves in shallow water with ambient currents. *Coastal Engineering*, 13(1), 23-54.

INNOCENTINI, V., ARANTES, F. O., FERREIRA, R. J. & MICHELETO, R. G. 2005. A agitação marítima no litoral Nordeste do Brasil associada aos distúrbios africanos de leste. *Revista Brasielira de Meteorologia*, 20(3), 367-374.

JOKIEL, P. L. 1978. Effects of water motion on reef corals. *Journal of Experimental Marine Biology and Ecology*, 35(1), 87-97, DOI: https://doi.org/10.1016/0022-0981(78)90092-8

KENCH, P. S. 1998a. A currents of removal approach for interpreting carbonate sedimentary processes. *Marine Geology*, 145(3-4), 197-223, DOI: https://doi.org/10.1016/S0025-3227(97)00101-1

KENCH, P. S. 1998b. Physical processes in an Indian Ocean atoll. *Coral Reefs*, 17, 155-168, DOI: https://doi.org/10.1007/s003380050110

KENCH, P. S. & BRANDER, R. W. 2006a. Response of reef island shorelines to seasonal climate oscillations: South Maalhosmadulu atoll, Maldives. *Journal of Geophysical Research: Earth Surface*, 111(F1), F01001, DOI: https://doi.org/10.1029/2005JF000323

KENCH, P. S. & BRANDER, R. W. 2006b. Wave processes on coral reef flats: implications for reef geomorphology using Australian case studies. *Journal of Coastal Research*, 22(1), 209-223.

KENCH, P. S., BRANDER, R. W., PARNELL, K. E. & MCLEAN, R. F. 2006. Wave energy gradients across a Maldivian atoll: implications for island geomorphology. *Geomorphology*, 81(1-2), 1-17, DOI: https://doi.org/10.1016/j.geomorph.2006.03.003

KRAINES, B., SUZUKI, A., YANAGI, T., ISOBE, M., GUO, X. & KOMIYAMA, H. 1999. Rapid water exchange between the lagoon and the open ocean at Majuro Atoll due to wind, waves , and tide. *Journal of Geophysical Research: Oceans,* 104(C7), 15635-15653.

LOWE, R. J. & FALTER, J. L. 2015. Oceanic forcing of coral reefs. *Annual Review of Marine Science,* 7, 43-66, DOI: https://doi.org/10.1146/annurev-marine-010814-015834

LOWE, R. J., FALTER, J. L., BANDET, M. D., PAWLAK, G., ATKINSON, M. J., MONISMITH, S. G. & KOSEFF, J. R. 2005. Spectral wave dissipation over a barrier reef. *Journal of Geophysical Research: Oceans*, 110(C4), C04001, DOI: https://doi.org/10.1029/2004JC002711

LOWE, R. J., FALTER, J. L., MONISMITH, S. G. & ATKINSON, M. J. 2009a. A numerical study of circulation in a coastal reef-lagoon system. *Journal of Geophysical Research: Oceans*, 114(C6), 1-18, DOI: https://doi.org/10.1029/2008JC005081

LOWE, R. J., FALTER, J. L., MONISMITH, S. G. & ATKINSON, M. J. 2009b. Wave-driven circulation of a coastal reef-lagoon system. *Journal of Physical Oceanography*, 39(4), 873-893, DOI: https://doi.org/10.1175/2008JPO3958.1

LUGO-FERNÁNDEZ, A., ROBERTS, H. H. & WISEMAN JUNIOR, W. J. 1998. Tide effects on wave attenuation and wave set-up on a Caribbean coral reef. *Estuarine, Coastal and Shelf Science*, 47(4), 385-393, DOI: https://doi.org/10.1006/ecss.1998.0365

MANDLIER, P. G. & KENCH, P. S. 2012. Analytical modelling of wave refraction and convergence on coral reef platforms: implications for island formation and stability. *Geomorphology*, 159-160, 84-92, DOI: https://doi.org/10.1016/j.geomorph.2012.03.007

MCGREGOR, G. R. & NIEUWOLT, S. 1998. *Tropical climatology — an introduction to the climates of the low latitudes.* 2nd ed. New York: Wiley.

NAKAMORI, T., SUZUKI, A. & IRYU, Y. 1992. Water circulation and carbon flux on Shiraho coral reef of the Ryukyu Islands, Japan. *Continetal Shelf Research*, 12(7-8), 951-970.

NELSON, R. C. 1996. Hydraulic roughness of coral reef platforms. *Applied Ocean Research*, 18, 265-274, DOI: https://doi.org/10.1016/S0141-1187(97)00006-0

PIANCA, C., MAZZINI, P. L. F. & SIEGLE, E. 2010. Brazilian offshore wave climate based on NWW3 reanalysis. *Brazilian Journal of Oceanography*, 58(1), 53-70.

ROBERTS, H. H., WILSON, P. A. & LUGO-FERNÁNDEZ, A. 1992. Biologic and geologic responses to physical processes: examples from modern reef systems of the Caribbean-Atlantic region. *Continental Shelf Research*, 12(7-8), 809-834, DOI: https://doi.org/10.1016/0278--4343(92)90046-M

SAHA, S., MOORTHI, S., PAN, H. L., WU, X., WANG, J., NADIGA, S., TRIPP, P., KISTLER, R., WOOLLEN, J., BEHRINGER, D., LIU, H., STOKES, D., GRUMBINE, R., GAYNO, G., WANG, J., HOU, H. T., CHUANG, H. Y., JUANG, H. M. H., SELA, J., IREDELL, M., TREADON, R., KLEIST, D., VAN DELST, P., KEYSER, D., DERBER, J., EK, M., MENG, J., WEI, H., YANG, R., LORD, S., VAN DEN DOOL, H., KUMAR, A., WANG, W., LONG, C., CHELLIAH, M., XUE, Y., HUANG, B., SCHEMM, J. K., EBISUZAKI, W., LIN, R., XIE, P., CHEN, M., ZHOU, S., HIGGINS, W., ZOU, C. Z., LIU, Q., CHEN, Y., HAN, Y., HIGGINS, W., ZOU, C. Z., LIU, Q., CHEN, Y., HAN, Y., CUCURULL, L., REYNOLDS, R. W., RUTLEDGE, G. & GOLDBERG, M. 2010. The NCEP climate forecast system reanalysis. *Bulletin of the American Meteorological Society*, 91(8), 1015-1057, DOI: https://doi.org/10.1175/2010BAMS3001.1

SMITHERS, S. G. & HOEKE, R. K. 2014. Geomorphological impacts of high-latitude stormwaves on low-latitude reef islands — observations of the December 2008 event on Nukutoa, Takuu, Papua New Guinea. *Geomorphology*, 222, 106-121.

SØRENSEN, O. R., KOFOED-HANSEN, H., RUGBJERG, M. & SØRENSEN, L. S. 2004. A third-generation spectral wave model using an unstructured finite volume technique. *In: Proceedings of the 29th International Conference on Coastal Engineering (ICCE).* Lisbon, Portugal, 19-24 Sep 2002. Lisbon: ICCE, pp. 894-906.

TARTINVILLE, B., DELEERSNIJDER, E. & RANCHER, J. 1997. The water residence time in the Mururoa atoll lagoon: sensitivity analysis of a three-dimensional model. *Coral Reefs*, 16, 193-203.

TOLMAN, H. L. 2002. *User manual and system documentation of WAVEWATCH-III version 2.22*. Washington, DC: US Department of Commerce NOOA (National Oceanic and Atmospheric Administration).

WOODROFFE, C. D. & BIRIBO, N. 2011. Atolls. *In:* HOPLEY, D. (ed.). *Encyclopedia of Modern Coral Reefs: structure, form and process*. Netherlands: Springer, pp. 51-71.

YOUNG, I. R. 1999. Seasonal variability of the global ocean wind and wave climate. *International Journal of Climatology*, 19(9), 931-950, DOI: https://doi.org/10.1002/(SICI)1097-0088(199907)19:9<931::AID--JOC412>3.0.CO;2-O

Supplementary material

Table S1. Summary of the maximum annual significant offshore wave heights (Hs) and peak period (Tp), with the associated hemisphere of incidence; and maximum annual offshore peak periods (Tp) and annual significant wave heights (Hs), with the associated hemisphere of incidence.

Offshore											
Maximum annual Hs						Maximum annual Tp					
Year	Month	Hs (m)	Tp (s)*	D*	Tide (m)	Year	Month	Tp (s)	Hs (m)*	D*	Tide (m)
1980	8	3.45	8.35	S	1.53	1980	2	20.26	1.7	N	1.66
1981	5	3.43	12.27	S	0.36	1981	3	20.35	2.34	S	2.1
1982	2	3.93	16.19	N	1.12	1982	4	20.33	1.99	S	1.64
1983	12	3.47	17.81	N	1.94	1983	12	19.84	2.04	N	1.25
1984	11	3.09	15.61	S	1.37	1984	8	20.42	1.99	S	1.47
1985	2	3.5	15.72	N	1.44	1985	2	21.21	1.68	N	0.38
1986	6	3.24	8.98	S	1.85	1986	12	19.06	1.85	S	1.9
1987	12	2.9	15.22	N	1.98	1987	2	21.79	2.28	N	1.62
1988	7	3.49	9.64	S	0.99	1988	11	20.58	2.15	N	0.53
1989	5	3.06	12.36	S	1.46	1989	6	20.06	1.75	S	2.3
1990	6	3.05	8.83	S	0.6	1990	11	19.74	2.19	N	1.75
1991	8	3.75	9.84	S	2.12	1991	1	19.63	2.78	N	0.4
1992	9	3.19	9.86	S	1.35	1992	9	18.5	1.91	S	1.82
1993	7	3.1	8.36	S	0.23	1993	3	18.97	2.25	N	0.58
1994	7	2.97	15.47	S	1.25	1994	12	19.11	1.59	N	0.6
1995	7	3.34	10.21	S	2.05	1995	8	18.83	2.24	S	0.27
1996	9	3.86	11.45	S	0.45	1996	1	20.03	2.27	N	1.78
1997	8	3.07	8.84	S	0.09	1997	12	21.03	1.39	N	0.2
1998	8	3.03	10.55	S	2.03	1998	11	20.37	1.83	S	1.54
1999	8	3.59	15.38	S	0.9	1999	1	20.94	1.97	N	2.16
2000	9	3.27	11.72	S	0.49	2000	12	19.11	2.02	N	1.85
2001	8	3.15	12.79	S	2.03	2001	2	18.5	2.58	N	-0.01
2002	8	3.7	10.93	S	0.59	2002	3	20.72	1.77	S	1.3
2003	7	3.02	9.76	S	2.01	2003	11	21.23	1.9	N	1.78
2004	8	3.31	11.07	S	1.56	2004	8	19.02	2.17	S	2.04
2005	7	3.2	13.52	S	1.25	2005	10	19.95	2.01	N	0.28
2006	7	3.63	9.83	S	1.8	2006	3	18.55	1.66	N	-0.01
2007	8	3.54	10.27	S	0.45	2007	1	19.31	1.5	N	1.72
2008	8	3.57	11.31	S	1.45	2008	9	18.77	2.44	S	1.08
2009	12	3.19	16.59	N	0.63	2009	5	19.82	1.52	S	2.28
2010	9	3.51	10.28	S	0.4	2010	2	19.62	1.79	N	2.36
2011	8	3.66	15.56	S	2.1	2011	5	17.82	2.16	S	1.8
2012	8	3.54	10.35	S	1.46	2012	7	19.27	2.18	S	2.15
2013	8	3.41	16.96	S	0.44	2013	12	20.29	2.31	N	1.82
2014	5	3.37	17.6	S	1.75	2014	8	20.14	2.25	S	2.13

Table S2. Summary of the maximum annual significant lagoon wave heights (Hs) and peak period (Tp), with the associated hemisphere of incidence; and maximum annual offshore wave peak periods (Tp) and annual significant wave heights (Hs), with the associated hemisphere of incidence.

Lagoon											
Maximum annual Hs						**Maximum annual Tp**					
Year	**Month**	**Hs (m)**	**Tp (s)***	**D***	**Tide (m)**	**Year**	**Month**	**Tp (s)**	**Hs (m)***	**D***	**Tide (m)**
1980	9	0.73	8.10	N	2.73	1980	2	12.39	0.31	N	1.66
1981	3	0.81	11.84	S	2.65	1981	2	12.32	0.59	S	2.22
1982	2	0.75	9.89	S	2.57	1982	4	12.16	0.12	N	1.04
1983	1	0.68	7.51	N	2.65	1983	12	12.13	0.22	N	1.25
1984	10	0.66	7.56	S	2.60	1984	12	12.03	0.19	N	1.07
1985	2	0.73	12.20	N	2.54	1985	7	12.47	0.13	N	1.13
1986	11	0.62	8.56	S	2.46	1986	3	11.46	0.25	N	1.38
1987	2	0.79	11.12	S	2.65	1987	2	13.32	0.34	N	1.62
1988	2	0.78	9.76	N	2.76	1988	11	12.06	0.28	N	1.46
1989	3	0.72	9.06	N	2.71	1989	9	11.65	0.14	N	1.22
1990	2	0.72	10.54	S	2.58	1990	11	11.90	0.36	N	1.75
1991	1	0.77	11.32	S	2.59	1991	1	11.84	0.20	N	1.24
1992	1	0.75	10.72	S	2.68	1992	4	10.96	0.33	N	1.69
1993	10	0.68	7.68	N	2.62	1993	9	11.14	0.20	N	1.25
1994	2	0.76	10.03	S	2.65	1994	12	11.55	0.23	N	1.41
1995	1	0.74	10.61	N	2.64	1995	3	11.03	0.20	N	1.20
1996	1	0.72	9.60	N	2.67	1996	1	12.17	0.39	N	1.78
1997	3	0.70	7.44	N	2.72	1997	12	12.26	0.16	N	1.00
1998	3	0.70	7.47	N	2.70	1998	11	12.29	0.12	N	1.07
1999	10	0.80	11.94	N	2.63	1999	1	12.87	0.55	S	2.16
2000	1	0.68	7.86	S	2.61	2000	12	11.60	0.39	N	1.85
2001	2	0.81	11.50	N	2.70	2001	2	11.50	0.81	N	2.70
2002	10	0.73	8.72	N	2.71	2002	3	12.18	0.14	N	1.30
2003	4	0.74	9.41	N	2.67	2003	11	12.89	0.37	N	1.78
2004	1	0.70	9.07	S	2.58	2004	1	11.17	0.25	N	1.40
2005	10	0.72	10.76	S	2.54	2005	10	11.87	0.24	N	1.36
2006	3	0.77	10.71	N	2.71	2006	3	10.75	0.18	N	1.14
2007	2	0.74	9.48	N	2.70	2007	1	11.82	0.21	N	1.34
2008	1	0.65	8.60	S	2.56	2008	9	11.10	0.13	N	1.08
2009	2	0.72	8.61	N	2.66	2009	5	11.60	0.11	N	1.16
2010	1	0.72	7.30	S	2.74	2010	2	11.99	0.60	S	2.36
2011	2	0.73	8.55	N	2.74	2011	1	10.74	0.22	N	1.33
2012	2	0.68	9.88	S	2.56	2012	1	10.78	0.21	N	1.34
2013	3	0.69	9.95	S	2.51	2013	12	12.34	0.48	N	2.01
2014	1	0.70	7.52	N	2.71	2014	1	11.51	0.68	N	2.53

* Associated values to Hs and Tp.